

Two-Dimensional Tungsten Photonic Crystals as Thermophotovoltaic Selective Emitters

Natalija Jovanović, Ivan Čelanović, Prof. John Kassakian

*Laboratory for Electromagnetic and Electronic Systems
Massachusetts Institute of Technology
77 Massachusetts Ave., Room 10-171, Cambridge, MA 02139, USA
Corresponding Author: Natalija Jovanovic, natalija@mit.edu*

Abstract. In this work we present the design, fabrication and characterization of photonic crystals (PhC) as selective thermal emitters for thermophotovoltaic (TPV) applications. The focus of our investigation is the development of thermal emitters based on two-dimensional (2D) PhC in single-crystal tungsten. We show that controlled periodic patterning can be used to fashion selective tungsten emitters that are well-matched to the photovoltaic (PV) diode of the system. The simulated emittance comparison of flat single-crystal tungsten and patterned single-crystal tungsten indicates potential for nearly doubling the TPV system efficiency. Measured results of a fabricated prototype structure correspond well to the simulated values. The fabrication is accomplished using laser interference lithography and reactive ion etching, the benefits and parameters of which are presented.

Keywords: Thermophotovoltaic, selective emitter, tungsten, photonic crystal

PACS: 78.20.Ci, 44.40.+a, 42.70.Qs, 42.72.Ai

INTRODUCTION

The direct conversion of thermal radiation into electricity is known as TPV power conversion. This technology has been investigated since the late 1950's [1-5], but has not seen extensive commercialization to date. The main obstacles to commercialization the systems' low efficiency and high cost. In order to achieve higher TPV efficiencies it is necessary to better match the radiated emitter spectrum to the sensitivity spectrum of the PV diode [6]. Spectral control component design and low-bandgap PV diode development have been the objectives of much research. Several selective emitter technologies have been under intense investigation, including rare-earth compounds, transition metal, and various micro-patterned structures [7].

Our research proposes a dual-spectral control TPV system that has the potential to drastically increase current TPV system efficiencies. In our proposed system, spectral control is achieved by a simple, yet highly-efficient one-dimensional (1D) PhC selective mirror and by a nanofabricated 2D PhC selective emitter. The selective mirror fabrication process and performance results are available in [8], while emitter fabrication and performance are presented in the remainder of this paper. The emitter fabrication process

meets dimensional precision requirements, while offering a substantial time-savings compared to many other fabrication methods. The process's simplicity, affordability, and equipment availability make it suitable for industrial applications.

MATERIALS, DESIGN DECISIONS, AND SIMULATIONS

Because of its high melting temperature, and its optical and structural properties, single-crystal tungsten (W) is the choice of substrate in this research. The refractive index of tungsten provides for increased normal emittance at wavelengths shorter than $2\mu\text{m}$, and suppressed emittance at longer wavelengths. Figure 1 shows normal emittance from a flat surface of single-crystal tungsten at room temperature. Refractive index values from [9] were used for this simulation. These emittance properties make tungsten particularly suitable for TPV applications using gallium antimonide (GaSb) PV cells, the band-gap energy of which corresponds to $1.78\mu\text{m}$ in wavelength.

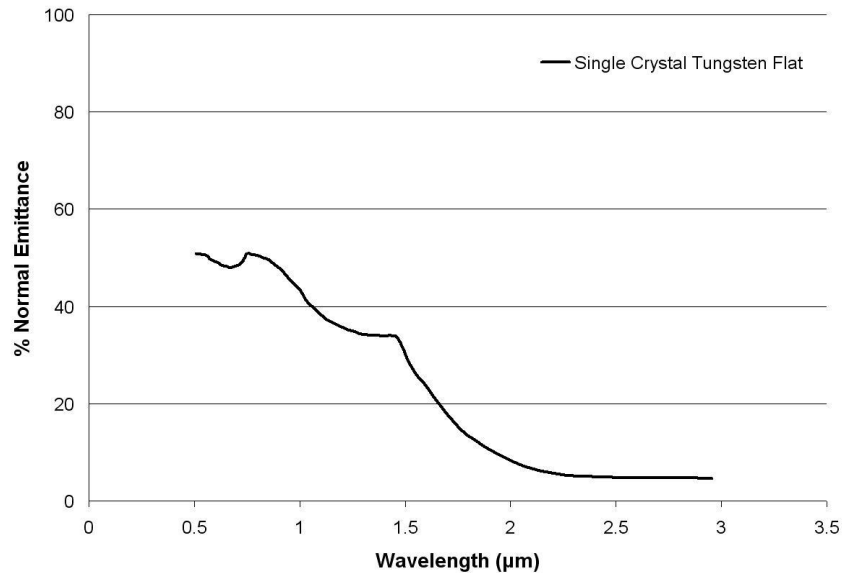


FIGURE 1. Single-crystal tungsten is a transition metal that naturally exhibits some selective emittance properties. Simulated normal emittance from a flat surface of single-crystal tungsten is shown.

Introduction of a properly-chosen periodic pattern of cavities can further increase the inherent selective emittance properties of tungsten. The cavities can be thought of as a cylindrical metallic waveguides, characterized by a unique dispersion relationship. More rigorous analysis of the structure was performed using the finite element method electromagnetic software package HFSS [10].

For this research, the chosen pattern consists of round cavities 800nm in diameter, in a 1000nm periodic pattern. The normal emittance of such a structure at room-temperature is shown in Figure 2. The simulation was done for infinitely deep holes. The suitability of

such structure's radiation properties for GaSb diodes is clear: the convertible energy (up to $1.78\mu\text{m}$) strongly outweighs the remainder of the spectrum.

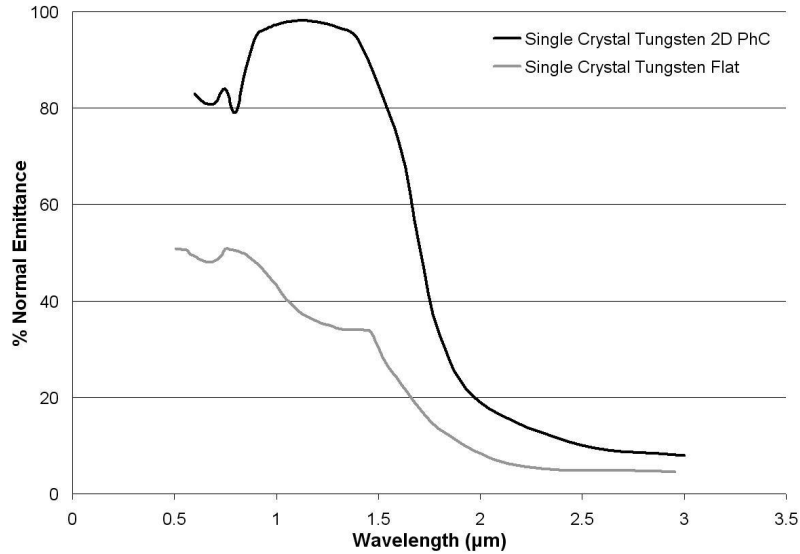


FIGURE 2. Introduction of a periodic pattern into single-crystal tungsten surface can greatly enhance the material's inherent selective emittance properties. Simulated normal emittance for a structure consisting of infinitely-deep, 800nm round holes in a 1000nm periodic pattern is shown.

SELECTIVE EMITTER PERFORMANCE

The sample produced for this research is a 2D PhC in single-crystal tungsten, with round holes 900nm in diameter and 560nm in depth. Figure 3 shows scanning electron (SEM) and atomic force micrographs (AFM) of the sample, respectively.

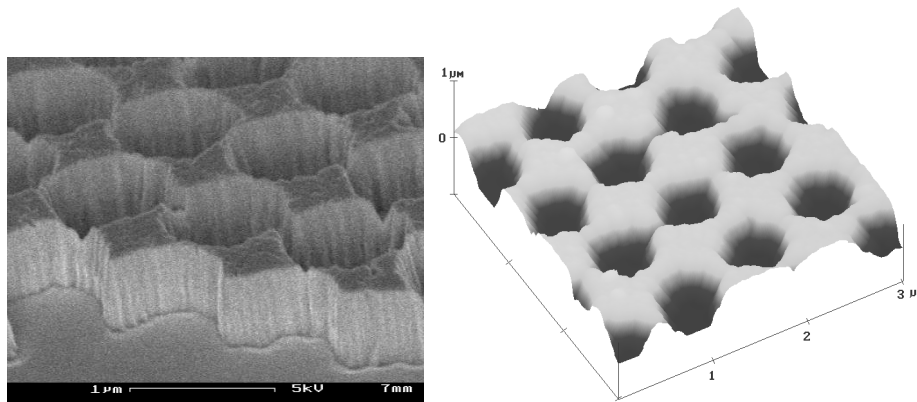


FIGURE 3. Tungsten 2D PhC selective emitter surface: scanning electron micrograph near sample edge (left) and atomic force micrograph (right). Some shape irregularities are pronounced due to proximity to the sample edge where defects tend to occur.

The room-temperature reflectance measurements at normal and oblique incidence were conducted using a Cary dual-beam spectrophotometer. Figure 4 shows emittance values for our sample, estimated from the reflectance measurements using the Kirchoff's law. Emittance is very high for wavelengths below 1.9 μm , which is very near the GaSb band-gap energy cut-off wavelength of 1.78 μm . Also, the sample largely maintains its selective emittance properties for all incident angles at which the measurements were conducted.

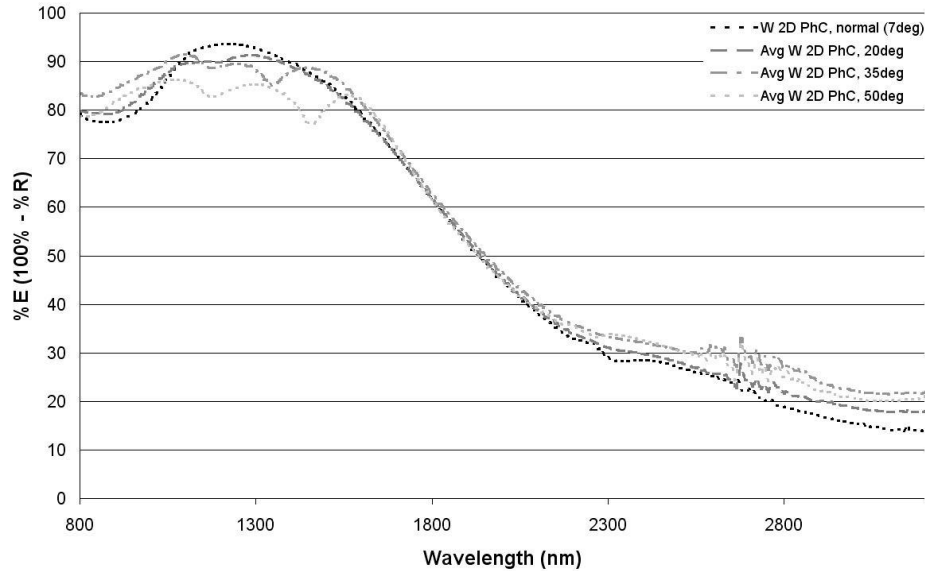


FIGURE 4. Tungsten 2D PhC emittance values measured using Cary spectrophotometer, for near-normal and oblique incident angles. The selective emittance properties are largely preserved over a broad range of incident angles.

It should be noted that the simulated structure had infinitely deep and perfectly round 800nm in diameter holes. The fabricated sample, however, had 900nm wide roughly round holes, that are only 560nm deep. Hence, some disagreement between the measurement and the simulation values is inevitable. Two areas of disagreement between the simulated and measured results are evident in Figure 4. Firstly, in the 800-1500nm wavelength range the emittance is lower than expected, which is mainly due to surface roughness and dimensional disparity between the simulated and fabricated structures. Dimensional disparity and substrate properties are the causes of disagreement in the 2000-3300nm wavelength range. In this range, the fabricated sample emits more than the simulated structure. The refractive index of the substrate used for fabrication is actually higher than the reference values used in simulation (Figure 5). An improvement to the emittance properties can be achieved by fabricating a more precise structure. Some alternative processing techniques are considered at the end of the next section.

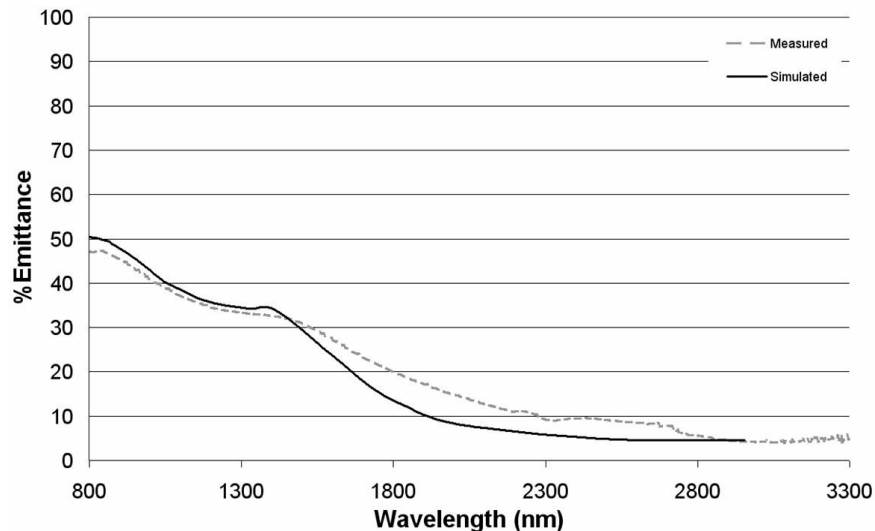


FIGURE 5. Single-crystal tungsten reflectance as measured and as simulated from reference values.

The room-temperature reflectance measurements of our 2D PhC tungsten selective emitter and measurements of the selective mirror transmittance were used to estimate the overall spectral efficiency. The radiated-transmitted spectrum for this dual spectral control technique is shown in Figure 6. In this manner, 93% of the spectrum is convertible by GaSb diodes.

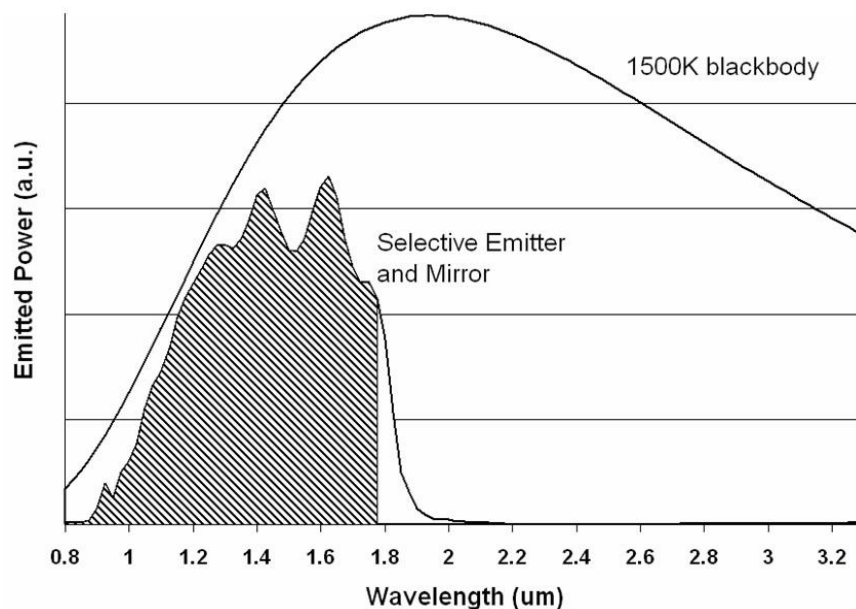


FIGURE 6. Spectrum resulting from combining 1500K blackbody radiation, the emittance of the selective emitter, and the transmittance of the 1D PhC selective mirror. In the resulting spectrum, over 90% of the power (shaded area) is convertible below the cut-off wavelength of GaSb diodes.

SAMPLE FABRICATION

The samples were produced using laser interference lithography (LIL). LIL facilitates fabrication of periodic structures with small-scale elements over large areas with relatively inexpensive and simple equipment. A single-wavelength light-source LIL can create a range of patterns and periods that exceed the capabilities of much more complicated stepper systems [11]. LIL systems are fast, exhibit excellent pattern coherence across large areas of exposure, and can achieve resolution comparable to stepper and electron-beam lithography systems.

The chosen fabrication process consists of two major parts: laser interference lithography (LIL) and reactive ion etching (RIE). The flow of the process is presented in Figure 7. The sample preparation starts with the deposition of the chromium (Cr), anti-reflective coating (ARC) and photoresist (PR) layers.

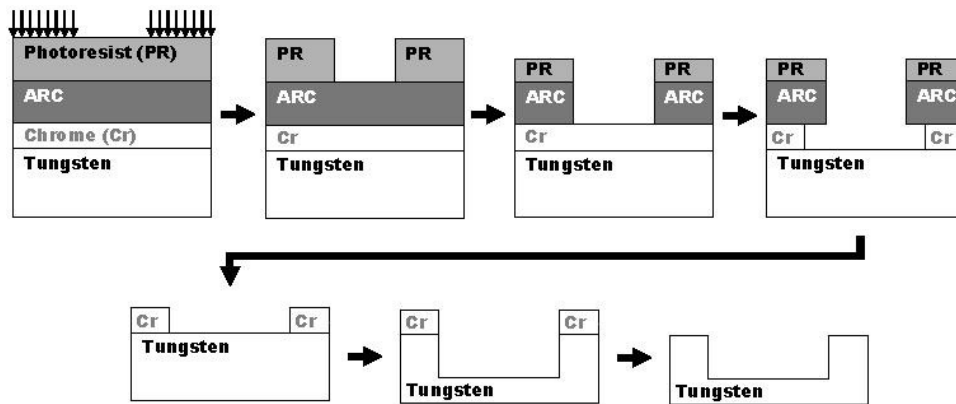


FIGURE 7. Tungsten 2D PhC selective emitter microfabrication process flow: lithography, development, ARC etch, chromium etch, photoresist and ARC removal, tungsten etch, and finally, chromium removal.

Lithography Process

LIL works on the principle of interfering coherent light waves. A light wave incident at an oblique angle can be decomposed into a perpendicular and a parallel component with respect to the sample surface. The interference of two coherent light waves parallel to the sample surface will create a grating pattern – alternating stripes of high and low intensity – that can be captured using photoresist. In this case the photoresist is THMR-iNPS4[®], supplied by OHKA America.

A square pattern of holes is achieved by exposing the sample twice and setting the angle between the exposures to 90° (Figure 8). For this process, the exposures are done at the same incident angle and for the same amount of time in each direction. The same incident angle results in the same periodicity of the two exposures. The same amount of time for each exposure results in the same duty cycle of the gratings.

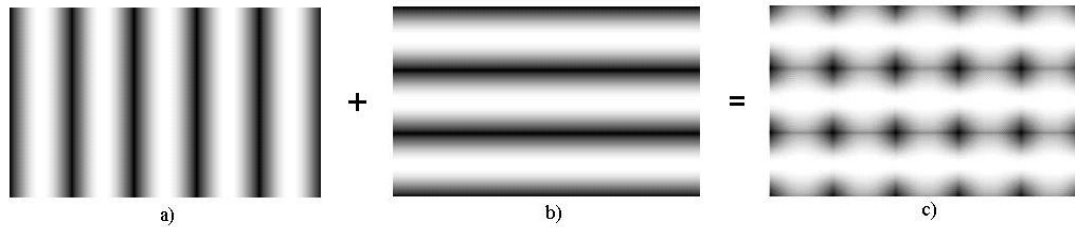


FIGURE 8. A square pattern of round holes (c) is achieved by two orthogonal LIL exposures (a, b).

Just like the interference of the light waves parallel to the sample results in the horizontal patterning of the resist, so does the interference of the perpendicular components and the wave reflected from the surface of the hard-mask layer result in the vertical patterning of the photoresist walls. The vertical standing wave, if powerful enough, will result in vertically sinusoidal walls. To lessen the influence of the vertical patterning, we introduce a layer of anti-reflective coating (ARC) between the photoresist and the substrate. This layer absorbs the reflection from the hard-mask layer, and therefore minimizes the power of the vertical standing wave. The ARC layer enables fabrication of straight sidewalls in the photoresist, which in turn improves the resolution of the pattern. With proper thickness, the ARC layer can eliminate virtually all vertical patterning in the photoresist layer. The ARC in our case is cyclohexanone-based BARLi[®], manufactured by Hoechst Celanese Corporation. A comparison of lithography results with and without an ARC layer is given in Figure 9. Strong vertical scalloping is evident in the sample fabricated without the ARC layer (Figure 9, right).

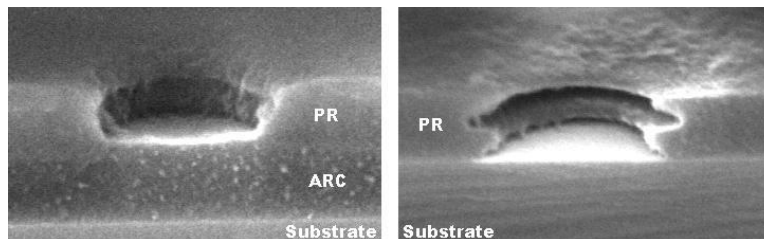


FIGURE 9. In LIL, interference of light wave components normal to the plane of the sample results in undesired “scalloping” in the photoresist (PR) layer (right). Anti-reflective coating (ARC) is used to minimize vertical interference and achieve more precise lithography results.

After the lithography step, the photoresist/ARC structure is baked to allow the photosensitive resin to cure. The pattern is developed using tetramethyl ammonium hydroxide (CD-26) developer by Shipley Company, Inc., then dried using gaseous nitrogen. The pattern is then transferred into the underlying ARC, Cr hard-mask and tungsten substrate by a sequence of etching processes.

Etching Process

After the lithography process, the structure consists of a patterned layer of photoresist and the underlying layers of ARC and hard-mask. The three-step etch process is described below.

Oxygen-based RIE is used to transfer the pattern from the photoresist into the ARC. The pattern is then transferred from the ARC layer into the chromium hard-mask layer by wet chemical etching. The chromium layer is etched using CR-7, a commercially available chromium etchant by Cyantek Corporation. Two characteristics of the fabrication process are very important to note at this point. Firstly, the holes in the chromium layer have a very large diameter-to-period ratio just as required by the preliminary simulations. Secondly, the holes are of very round and uniform shape just as required by the proposed structure.

In the final etch step, carbon-tetrafluoride-based RIE is used to transfer the pattern from the chromium hard-mask layer into the tungsten substrate (Figure 3). Most deviation from expected shape in the final structure results from the chromium wet-etch fabrication step. In this step, it is very difficult to control the radius of the etched holes due to the non-constant etch rates. It is also difficult to control the roughness of the hole edges due to granularity of the chromium layer.

One improvement to this step has already been investigated. Diluting the etching solution provides for more precise control of the hole radius. One other possibility is to use chlorine-enhanced RIE to etch the chromium layer. This process is more precise, but the equipment and the etch rates have yet to be characterized for our particular needs.

The roughness of the walls in the chromium layer is transferred into the tungsten layer during the tungsten RIE process. The RIE process accentuates these irregular shapes. However, because of their nanometer-scale average, the sidewall roughness features don't seem to significantly influence the structure's properties in the frequency range of interest.

Overall, the fabrication process produces the desired structure in a fast, simple, and relatively inexpensive manner. The fabrication techniques allow for a wide variety of patterns to be produced at no modification cost to the equipment.

CONCLUSIONS AND FUTURE WORK

We have investigated design, simulation, fabrication, and preliminary characterization of dual spectral control for TPV systems. By using two relatively simple and moderately efficient spectral control components, higher spectral efficiency can be achieved at lower cost and reduced complexity of individual components. The challenges that remain for future research include emitter pattern stability over temperature cycles and time, and therefore determination suitable operating temperature and possible lifetime. Also, implementation of inert operating atmosphere for the tungsten selective emitter will introduce a new complexity to the system.

Dual spectral control has potential to bring TPV system efficiencies significantly closer to their thermodynamic limit. With continued investigation into new materials and structures, TPV systems are coming closer to becoming a viable technology for a variety of power conversion applications.

ACKNOWLEDGMENTS

The authors would like to acknowledge Toyota Motor Corporation for supporting this research, and the MIT NanoStructures Laboratory for providing access to fabrication facilities. This work made use of MIT MRSEC Shared Facilities supported by the National Science Foundation under Award Number DMR-0213282.

REFERENCES

1. H. H. Kolm, "Solar-battery power source," Quarterly Progress Report, Solid State Research, Group 35, MIT-Lincoln Laboratory, Lexington, MA, pp. 13, 1956.
2. P. Aigrain, "The Thermophotovoltaic Converter," unpublished lectures given at the Ecole Normale Supérieure (1956), and the Massachusetts Institute of Technology, (1960-1961).
3. B. D. Wedlock, "Thermo-Photo-Voltaic Energy Conversion," *Proceedings IEEE* **51**, pp. 694-698 (1963).
4. G. Guazzoni and S. Matthews, "A Retrospective of Four Decades of Military Interest in Thermophotovoltaics" in *Thermophotovoltaic Generation of Electricity: 6th Conference*, edited by A. Gopinath, et. al., AIP Conference Proceedings 738, American Institute of Physics, Melville, NY, 2004, pp. 3.
5. R. E. Nelson, "TPV Systems and State-of-Art Development" in *Thermophotovoltaic Generation of Electricity: 5th Conference*, edited by T. J. Coutts, et. al., AIP Conference Proceedings 653, American Institute of Physics, Melville, NY, 2002, pp. 3.
6. G. W. Garache, et. al., "Design Issues in Thermophotovoltaic Systems" *Compound Semiconductor* **4**, no. 7 (1998).
7. A. Gombert, "An Overview of TPV Emitter Technologies" in *Thermophotovoltaic Generation of Electricity: 5th Conference*, edited by T. J. Coutts, et. al., AIP Conference Proceedings 653, American Institute of Physics, Melville, NY, 2002, pp. 123.
8. F. O'Sullivan, I. Celanovic, N. Jovanovic, S. Akiyama, K. Wada, and J. Kassakian, "Optical characteristics of one-dimensional Si/SiO₂ photonic crystals for thermophotovoltaic applications" *Journal of Applied Physics* **97**, p. 033529 (2005).
9. Lynch, D.W. and Hunter, W.R., *Handbook of Optical Constants of Solids I*, edited by Palik, E.D., New York: Academic Press, 1985, pp. 334-341.
10. *Ansoft High Frequency Structure Simulator Manual*. Pittsburgh, PA: Ansoft Corporation, 2001.
11. M. Walsh, "Nanostructuring Magnetic Thin Films Using Interference Lithography," M.S. Thesis, Department of Electrical Engineering and Computer Science, MIT, August 2000.